Source parameters and seismic moment-magnitude scaling for Northwestern Turkey.

Parolai S. [(1)], D. Bindi[(2)], E. Durukal[(3)] , H. Grosser[(1)], and C. Milkereit [(1)].

(1) GeoForschungsZentrum Potsdam, Telegrafenberg, 14473, Potsdam Germany

(2) Istituto Nazionale di Geofisica e Vulcanologia, via Bassini 15, 20133 Milano, Italy

(3) Bogazici University, Kandilli Observatory and Earthquake Research Institute, Department of Earthquake Engineering, 34684, Cengelkoy, Istanbul, Turkey

Abstract

The source parameters of 523 aftershocks ($0.5<M_L<5.9$) of the 1999 Kocaeli earthquake are determined by performing a two-step spectral fitting procedure. The source spectrum, corrected for both site and propagation effects, is described in terms of a standard ω-square model multiplied by an exponential term of frequency. The latter term is introduced to estimate the high frequency (f>12Hz) fall-off of the acceleration source spectra, by computing the κ parameter. The obtained seismic moments range between 1.05×10^{14} and 2.41×10^{17} Nm, while the Brune-stress drops are between 0.002 and 40 MPa. κ varies between 0.00 and 0.08 s indicating a decay of the acceleration level at high frequency greater than that assumed by the ω^{-2} model. Both the stress drop and the κ parameter show the tendency of increasing with aftershock magnitude. No evidence of self similarity break down is observed between the source radius and M_0. Finally, both the seismic moment and the moment magnitude are compared to the local magnitude to derive new moment-magnitude relationships for the area, to be considered for seismic hazard assessment.

Introduction

On August 17, 1999, a magnitude Mw=7.4 earthquake struck the Kocaeli province of Turkey and three months later, on November 12, 1999, the Mw=7.2 Düzce earthquake occurred to the immediate east of the fault rupture of the Kocaeli earthquake. Since then, many studies (among many others *Tibi et al*., 2001, *Eken et al*., 2004, *Durukal and Catalyürekli*, 2004, *Bindi et al*., 2006a, *Bindi et al*., 2006b) have focused on this area. Recent studies (e.g *Atakan et al*., 2002; *Erdik et al*., 2004; *Parsons*, 2004) showed that the segments of the North Anatolia Fault in the Sea of Marmara to the immediate south of Istanbul have a very significant probability (40-65%) of producing a M>7 earthquake within the next 30 years that will likely create very high hazard levels in the city of Istanbul. With the recognition of the substantial earthquake hazard and risk levels of Istanbul, many international projects have been initiated with the ultimate aim of mitigatiing urban earthquake risk. Within the framework of one of these, "Megacity Istanbul", one objective was to determine the actually lacking source parameter scaling relationships for the area that can then be used both for the simulation of regional strong ground motion (e.g. Boore, 2003) , and for seismic hazard predictions, using, for example a standard probabilistic approach (Cambiarla con Cornell? *Franceschina et al*., 2006). In fact, source parameters play a key role in the estimation of attenuation relationships, in the definition of source parameterization for ground motion simulation etc. (necessary?)

In this study, source parameters of 523 earthquakes recorded by two seismic networks (German Task Force – GTF and SApancaBOlu -SABO) and a strong motion network (Kandilli Observatory and Earthquake Research Institute -KOERI) are derived. The source spectrum was obtained by means of the generalized inversion technique (*Castro et al.*, 1990; *Bindi et al*., 2006a) and then fitted in a first step using a Brune-source model (*Brune*, 1970). The fit was also performed in a second step by introducing a high frequency diminution term (*Halldorsson and Papageorgiou*, 2005). The seismic

moment was used to derive new empirical relationships with the local magnitude M_L (calibrated for the area by *Baumbach et al.* (2003) and updated recently by *Bindi et al*., (2006c)). New empirical relationships between seismic moment and source radius, as well as between rms stress drop ($\Delta\sigma_{rms}$) (*Andrews*, 1986) and Brune stress drop ($\Delta\sigma_B$), are also shown. These relationships can be used to guide ground-motion predictions in the area.

Data

Amongst the aftershocks recorded by the 53 stations of the GTF, SABO and KOERI networks, the recordings of 523 earthquakes with M_L ranging between 0.5 and 5.9 were considered. GTF and SABO networks consist of 1-Hz geophones (Mark L4-3D), a 24-bit digitizer with a sampling rate of 100 sps and Global Positioning System (GPS) timing. The KOERI strong-motion network consist of GeoSys GSR-16 and Kinemetrics SSA-2 strong motion stations working with sampling rates of 200 sps.

The selection of the events was carried out aiming at obtaining satisfactory ray-path coverage (as requested from the generalised inversion technique) of the area from well-located events (Figure 1). The hypocenter locations of the selected earthquakes, calculated using a standard procedure (*Bindi et al.*, 2006c), lead to root mean squares (RMS) values of the travel time residuals smaller than 0.5 s, with an average value of 0.13 s. The horizontal and vertical statistical errors are smaller than 1.8 and 2 km, respectively.

For all recordings, the Fast Fourier Transform (FFT) of a 5s window of signal, starting 1 second before the S-wave arrival was calculated. If the difference between S- and P-wave arrival time was smaller than 1 second (check how many cases!) the window was shifted in order to avoid the main P-wave arrival energy. Trends from the chosen signal windows were removed, and a 5% cosine taper was applied at both ends before the

FFT calculation. Spectra were corrected for the instrumental response of the sensors and smoothed using a *Konno and Ohmachi* (1998) window with b= 20. Generally b is varied between 10 and 60 with the smaller values determining larger smoothing of the spectra. As a final step of data preparation, the vector sum of the two horizontal and vertical spectra was obtained. The reader is referred to *Baumbach et al*. (2003), *Parolai et al*. (2004), *Bindi et al.* (2006a) and *Bindi et al*. (2006b) for more detailed information about the data set.

Method

Source spectra were obtained by the generalized spectra inversion [e.g. *Castro et al*., 1990], that allows the separation of the site, path and source contributions from the observed spectra. This is achieved after having taken the logarithm of the spectra of the recordings – of several earthquakes registered by different stations- and solving the resulting linear system in a least-squares sense. A non-parametric approach was here adopted for the inversion. The distance range covered by the data set (10 to 190 km) was discretized into 60 bins with widths of 3 km. The inversion was performed separately for each of the 70 selected frequency, equi-spaced in logarithmic scale between 0.4 and 25 Hz, using the least square algorithm (LSQR) of Paige and Saunders (1982). A detailed description of the inversion can be found in *Parolai et al* .(2004) and *Bindi et al*. (2006a).

In order to derive source parameters like seismic moment, corner frequency and $\Delta\sigma_B$ a two-step procedure was followed.

In a first step, displacement source spectra were fitted to a ω-square source model with only one corner frequency (*Brune*, 1970), assuming an S-wave velocity of 3.5 km/s, a density of 2800 kg m^{-3} and an average radiation pattern of 0.6. A grid search procedure was applied, where $\Delta\sigma_B$ was varied between 1kPa and 100 MPa, and the seismic moment M_0 over intervals depending on the magnitude. The M_0 intervals ranged between 10^9 Nm

and 10^{12} Nm for the smallest analysed events and between 10^{16} Nm and 10^{18} Nm for the largest ones. In particular, 20 steps per decade (equally spaced in logarithmic scale) were allowed for both parameters. The cost function to minimize was

$$rms = \sqrt{\frac{\sum_{1}^{N_f} (\log O(f) - \log C(f))^2}{N_f}} \quad (1)$$

where $O(f)$ is the observed spectrum, $C(f)$ is the calculated spectrum, and N_f is the number of considered frequencies. The frequency range considered was 0.5-25 Hz. Although the spectral fit was generally very good (Figure 2, top panel), it was found that the high-frequency part of the source spectrum was not completely described by the adopted function, consistent with the generally observed rapid decay (greater than that assumed by ω^{-2} model) of the acceleration level at high frequency (*Hanks*, 1979; *Halldorsson and Papageorgiou*, 2005). Therefore, in a second step, acceleration source spectra were fitted by considering not only a ω-square model but also a high frequency diminution function (*Halldorsson and Papageorgiou*, 2005)

$$D(f, \kappa) = \exp(-\pi \kappa f) \quad (2)$$

Where f is the frequency, and, in this study, κ is a parameter determining the high frequency source spectral decay. It accounts for the source contribution (*Purvance and Anderson*, 2003) to the parameter κ, defined in *Anderson and Hough* (1984) that is generally adopted in stochastic simulations of strong ground motion. The second step constrains M_0 to the value calculated in step 1, and allows for a grid search for $\Delta\sigma_B$ and κ. After a visual inspection of all the fit results (or spectra?) of step 1, the function $D(f, \kappa)$ was applied from 12 Hz, which for this data set is where the high frequency decay generally begins. In the grid search procedure, $\Delta\sigma_B$ was varied between 1 kPa and 40 MPa in steps of 0.01 MPa, while κ was varied between 0.0 s and 0.1 s in steps of 0.002 s. The cost function was defined as in step 1. The excellent final fits (0.09 and 0.06)

obtained for two sample events with M_L 5.5 and 2.1, respectively, are shown in Figure 2, bottom panel.

Results

Before discussing into details the relationships between the parameters obtained form the two-step procedure, an inspection to the *rms* values (Figure 3) provides information on the accuracy of their estimation. The values are quite small, with the great majority being less than 0.2. Less accurate fits (*rms* >0.2) were obtained for higher magnitude events (M_L>3.5-4), indicating problems in the adopted procedure when the corner frequency (f_c) of the event is closer to the lower bound of the analysed frequency band. A strong reduction of *rms* reached after the second step when the fit was performed considering also κ is evident, confirming that the use of the high-frequency diminution function $D(f, \kappa)$ is appropriate. The average *rms* after the second step of the procedure decreases from 0.127±0.048 to 0.079±0.029.

The κ values range between 0.00 and 0.08 s, showing a clear tendency to increase with M_L. Note that the site and path effects were removed from the fitted source spectra by the generalized inversion technique. The positive correlation between κ and M_L (the best fitting, in a least-squares sense line has a slope equal to 0.0071±0.0005) agrees with the results obtained by Bindi et al (2006b), who inverted κ values estimated directly from the observed acceleration spectra, so as to isolate the site, source and path contributions, without introducing any source model. They also found that the source contribution to κ correlates with M_L, with the least-squares fit of the results giving a slope equal to 0.0051. The high scatter in the distribution of κ against M_L shown in Figure3, implies a correlation coefficient R=0.5086, with a null hypothesis of no-correlation between the two parameters that can be rejected at a 0.98 level of confidence by performing a t-Student test.

Figure 4 shows graphically the scaling between f_c and M_L and that between M_0 and the Brune source radius. A clear scaling of the corner frequency with M_L is observed within the full magnitude range considered ($0.5 < M_L < 5.9$). This is reflected in the scaling of the source radius versus the M_0, where the source radius varies from nearly 100 m to 2.5 km. Consistent with previous studies (e.g. *Abercombie*, 1995; *Franceschina et al.*, 2006) no evidence of self similarity break down is observed within the range of M_0 investigated ($1.05 \times 10^{14} < M_0 < 2.41 \times 10^{17}$ Nm). However, a tendency of $\Delta\sigma_B$ (varying between 2 kPa and 40 MPa, but with the great majority of values between 10 kPa and 10 MPa) to increase with M_0 is shown in Figure 4. The large scattering shown by the $\Delta\sigma_B$ values might be related to the hypocentral location and the focal mechanism.

The corner frequency and $\Delta\sigma_{rms}$ were calculated following Andrews (1986), in order to have an independent estimate of the stress drop. In this way, $\Delta\sigma_{rms}$ is calculated directly from the acceleration spectrum without making any assumption about the source function. For a case where the source spectrum is identical to a Brune model, $\Delta\sigma_{rms}$ should equal $\Delta\sigma_B$.

Figure 5 shows that $\Delta\sigma_B$ appears to be strongly correlated with $\Delta\sigma_{rms}$, where the average of the $\log_{10}$ of the spectral ratio between $\Delta\sigma_{rms}$ and $\Delta\sigma_B$ equals -0.19±0.37. Since the same ratio calculated using the $\Delta\sigma_B$ from step 1 (also showing a strong correlation with $\Delta\sigma_{rms}$) provided a value of 0.034 ±0.37, it appears that, as expected, the introduction of the κ factor leads to a shift toward higher values of $\Delta\sigma_B$.

Finally, in Figure 6, M_0 (top) and Mw (bottom), obtained using the equation of *Kanamori* (1977), are shown versus M_L. A linear orthogonal regression between $\log_{10} M_0$ and M_L (black line in Figure 6, top) led to the equation

$$\log_{10} M_0 = (1.17 \pm 0.01)\, M_L + (10.12 \pm 0.02) \qquad (3)$$

While this relationship is in good agreement with that of *Grosser et al.,* (1998) (gray line) calculated from the aftershocks of the Erzican earthquake, it differs to that of

Durukal and Catalyürekli, (2004) (dashed line). We believe that this disagreement may be due to the use of a M_L scale with coefficients not calibrated for the area in the latter study.

Results of the regression between Mw and M_L are shown in Figure 6, bottom. In this case, a non-linear least-squares regression was carried out considering a quadratic term. Since the regression is not orthogonal, it was carried out in two directions, considering in one case M_L, and in the other Mw, as independent variables. Therefore, two relationships obtained are:

$$Mw \leftarrow (0.95\pm0.03) + (0.58\pm0.02)M_L + (0.03\pm0.004)M_L^2 \quad (4)$$

$$M_L \leftarrow (-9.001\pm1.59) + \sqrt{((54.25\pm25.94) + (30.19\pm4.11)Mw)} \quad (5)$$

Since the data set shows a strong correlation between Mw and M_L with a very limited scattering of data points, indicating that path and site-effect corrections were efficiently carried out, both relations, when plotted, lead to very similar graphs. That is why in Figure 6, bottom, only equation (4) is shown. The new relationship shows generally a good agreement with the chi-square regression derived by *Stromeyer et al*. (2004) (gray line) for continental Europe. Small discrepancies may be due to the different tectonic regimes of the areas in which the data sets have been collected.

Conclusions

New source spectral models for Northwestern Turkey have been calibrated using a large data set of aftershocks (523) following the Kocaeli earthquake. The main results are summarized as follows:

- Introducing a high frequency diminution function improved the spectral fit with respect to that obtained considering only a Brune source model.

- The obtained values of κ appear to vary as a function of M_L. The null hypothesis of no-correlation between the two parameters can be rejected at a 0.98 level of confidence by performing a t-Student test.
- $\Delta\sigma_B$ appears to increase with Mo in the analyzed seismic moment range ($1.05 \times 10^{14} < M_0 < 2.41 \times 10^{17}$ Nm).
- $\Delta\sigma_B$ and $\Delta\sigma_{rms}$ appear to be strongly correlated, indicating that the source spectra can be correctly describe by a Brune source model, and that the estimate of f_c are reliable.
- New relationships between M_L, calibrated for the first time in the area by *Baumbach et al.*, (2003) and updated by *Bindi et al.* (2006c), and Mw, were derived.

The large scattering shown by the $\Delta\sigma_B$ values might be related to the hypocentral location and the focal mechanism. This point will be subject of future investigations.

The new relationships provide important information about source parameters such as $\Delta\sigma_B$ and κ, and thus can assist efforts to simulate strong ground motion in northwestern Turkey.

Acknowledgments

This work was partially funded by the project “Megacity: Istanbul". Part of this work was conducted during the visits of Dino Bindi at the GFZ-Potsdam that were partially funded by the GeoForschungsZentrum Potsdam. K. Fleming kindly improved our English. We thank M. Bohnhoff and E. Gorgun, for having provided part of the arrival time pickings and the earthquake locations. Figures were generated using the Generic Mapping Tools (Wessel and Smith, 1991).

232 **References**

233 Abercombie, R.E., (1995). Earthquake source scaling relationships from -1 to 5 M_L
234 using seismograms recorded at 2.5 km depth, *J. Geophys, Res*., 100, 24015-24036.
235
236 Anderson, J. G., and S. E. Hough (1984). A model for the shape of the Fourier amplitude
237 spectrum of acceleration at high frequencies, *Bull. Seism. Soc. Am*., 74, 1969-1993.
238
239 Andrews, D. J. (1986). Objective determination of source parameters and similarity of
240 earthquakes of different size, In: Das, S., Boatwrigth, J., Scholz, C.H. (Eds.), *Earthquake*
241 *source mechanics*, Am. Geophys. Union, Geophys. Monogr., 37,vol. 6, 259-267.
242
243 Atakan, K., A. Ojeda, M. Meghraoui, A. A. Barka, M. Erdik, and A. Bodare, (2002).
244 Seismic Hazard in Istanbul following the 17 August Izmit and 12 November 1999 Düzce
245 earthquakes, *Bull. Seism. Soc. Am*., 92, 1, 466-482.
246
247 Baumbach, M., D. Bindi, H. Grosser, C. Milkereit,S. Parolai, R. Wang, S. Karakisa, S.
248 Zünbül, and J. Zschau (2003). Calibration of an M_L scale in Northwetsren Turkey from
249 1999 Izmit aftershocks, *Bull. Seism. Soc. Am*., 93, 5, 2289-2295.
250
251 Bindi D., S. Parolai, H. Grosser, C. Milkereit, and S. Karakisa, (2006a). Crustal
252 attenuation characteristics in northwestern Turkey in the range from 1 to 10 Hz, *Bull.*
253 *Seism. Soc. Am*., 96, 200-214.
254
255 Bindi D., S. Parolai, H. Grosser, C. Milkereit, and S.Zümbül, (2006b). Cumulative
256 attenuation along source-to-receiver paths in northwestern Turkey, *Bull. Seism. Soc. Am*.,
257 96, 188-199.

Bindi D., S. Parolai, E. Görgün, H. Grosser, C. Milkereit, M. Bohnhoff, E. Durukal, (2006c). M_L scale in Northwestern Turkey from 1999 Izmit aftershocks: updates, submitted to *Bull. Seism. Soc. Am.*

Boore, D., (2003). Simulation of ground motion using stochastic method, *Pure Appl., Geophys*., 160, 635-676.

Brune, J. N. (1970). Tectonic stress and the spectra of seismic shear waves from earthquakes, *J. Geophys. Res*., 75, 4997-5009.

Castro R.R., J.G. Anderson, and S.K Singh (1990). Site response attenuation and source spectra of S waves along the Guerrero, Mexico, subduction zone, *Bull. Seism. Soc. Am*., 80, 1481-1503.

Durukal E., and Y. Catalyürekly (2004). Spectral analysis of source parameters of the 1999 Kocaeli and Düzce earthquake aftershock sequences, *13th WCEE*, Vancouver, B.C., Canada, August 1-6, 2004, Paper n. 421.

Eken, T., K. Mayeda, A. Hofstetter, R. Gök, G. Örgülü, and N. Turkelli (2004). An application of the coda methodology for moment-rate spectra using broadband stations in Turkey, *Geophys. Res. Lett.*, 31, L11609, doi:10.1029/2004GL019627.

Erdik, M., M. Demircioglu, K. Sesetyan, E. Duruka, B. Siyahi (2004). Earthquake hazard in Marmara region, Turkey, *Soil. Dynam. Earthquake Eng*., 24, 605-631.

Franceschina G., S. Kravanja and G. Bressan, (2006). Source parameters and scaling relationships in the Friuli-Venezia Giulia (Northwestern Italy) region, *Phys. Earth Plan. Int.*, 154, 148-167.

Grosser, H., and other 11 co-authors, (1998). The Erzican (Turkey) earthquake (Ms 6.8) of March 13, 1992 and its aftershocks sequence, *Pure Appl., Geophys*., 152, 465-505.

Halldorsson, B., A. S. Papageorgiou (2005). Calibration of the specific barrier model to earthquakes of different tectonic regions, *Bull. Seism. Soc. Am*., 95, 4, 1276-1300.

Hanks, T., (1979). *b* values and $\omega^{-\gamma}$ seismic source models: implications for tectonic stress variations along active crustal fault zones and the estimation of high-frequency strong ground motion. *J. Geophys. Res*., 84, 2235-2242.

Kanamori, H., (1977). The energy release of great earthquakes, *J. Geophys., Res*., 82, 2981-2987.

Konno, K., and T. Ohmachi (1998). Ground-motion characteristic estimated from spectral ratio between horizontal and vertical Components of Microtremor, *Bull. Seism. Soc. Am*., 88, 228-241.

Paige, C. C., and M. A. Saunders (1982). An algorithm for sparse linear equations and sparse least squares, *ACM Trans. Math. Soft.,* **8,** 43-71.

Parolai, S., D. Bindi., M. Baumbach, H. Grosser., C. Milkereit, S. Karakisa, S. Zünbül (2004). Comparison of different site response techniques using aftershocks of the 1999 Izmit earthquake, *Bull. Seism. Soc. Am*., 94, 1096-1108.

Parsons, T. (2004). Recalculated probability of M≥7 earthquakes beneath the Sea of Marmara, Turkey, *J. Geophys. Res.,* vol 109, B05304, doi:10.1029/2003JB002667.

Purvance, M. D., and J.G. Anderson (2003). A comprehensive study of the observed spectral decay in strong-motion accelerations recorded in Guerrero, Mexico, *Bull. Seism. Soc. Am*., 93, 600-611.

Stromeyer, D., G. Grünthal., and R. Wahlström, (2004). Chi-square regression for seismic strength parameter relations, and their uncertainties, with applications to an Mw based earthquake catalogue for central, northern and northwestern Europe, *J. of Seismology*, 8, 143-153.

Tibi, R., G. Bock, Y. Xia, M. Baumbach, H. Grosser, C. Milkereit, S. Karakisa, S. Zünbül, R. Kind, and J. Zschau (2001). Rupture process of the 1999 August 17 Izmit and November 12 Düzce (Turkey) earthquakes, *Geophys. J. Int*., 144, F1-F7.

Wessel, P., and W.H.F. Smith (1991). Free software helps map and display data, *EOS. Trans. AGU*, 72, 441, 445-446.

330 **Figure captions**

331

332 **Figure 1**: Top. Epicenter location (circles), seismological GTF and SABO (triangles) and
333 strong motion (KOERI) stations (squares). Bottom: Epicenter to seismic station ray paths
334 (black lines). Epicenter to strong-motion station ray paths (gray lines).

335

336 **Figure 2**: Top. Displacement spectra (black line) for M_L 5.5 and 2.1 earthquakes. The best fit
337 spectra obtained by the grid search procedure (step 1) are indicated by the gray lines.
338 Bottom. Acceleration spectra (black lines) for M_L 5.5 and 2.1 earthquakes. The best fit spectra
339 obtained by the grid search procedure (step 2) are indicated by the gray lines.

340

341 **Figure 3**: Top. κ values versus M_L. Bottom. *rms* versus M_L after step 1 (grey circles). *rms*
342 versus M_L after step 2 (black circles).

343

344 **Figure 4**: Top. f_c versus M_L. Bottom. $\log_{10}M_0$ versus source radius R. Line (black) of constant
345 $\Delta\sigma_B$ between 0.01 MPa (0.1 bar) and 10 MPa (100 bar) are shown.

346

347 **Figure 5**: $\Delta\sigma_{rms}$ versus $\Delta\sigma_B$.

348

349 **Figure 6**:Top. $\log_{10}M_0$ versus M_L (squares). Equation (3) from this study (black line), *Grosser*
350 *et al.,* (1998) (gray line), and *Durukal and Catalyürekli*, (2004) (dashed line). Bottom. Mw
351 versus M_L (squares) . Equation (4) from this study (black line), and *Stromeyer et al*. (2004)
352 (gray line).

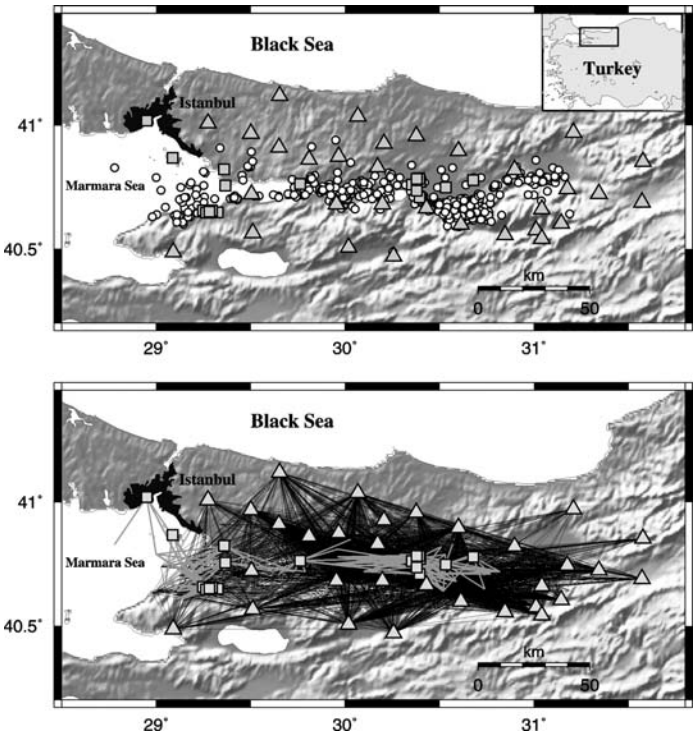

353

354

355 **Figure 1**:

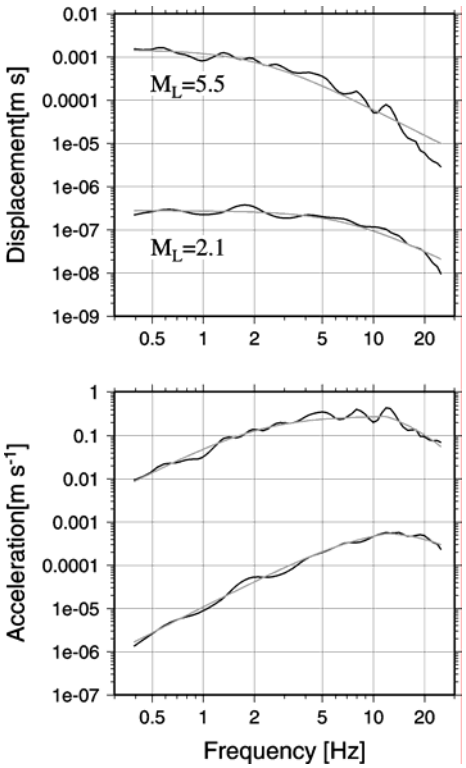

Figure 2.

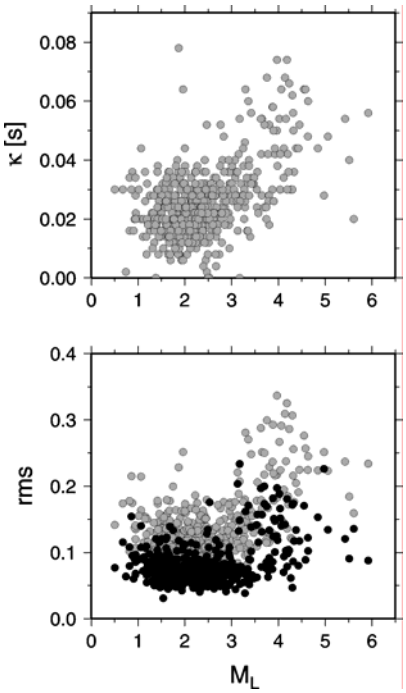

Figure 3.

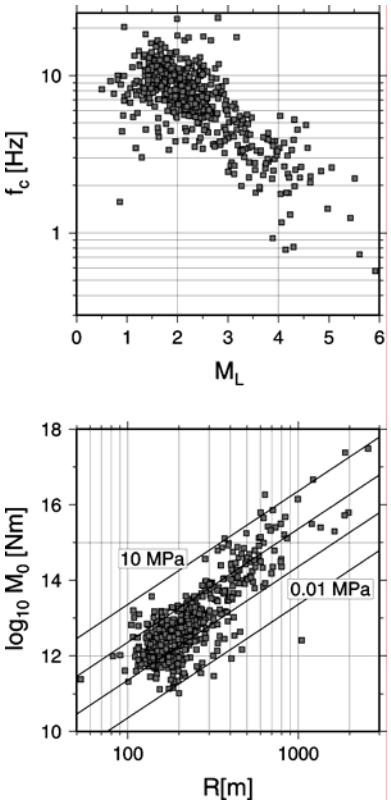

Figure 4.

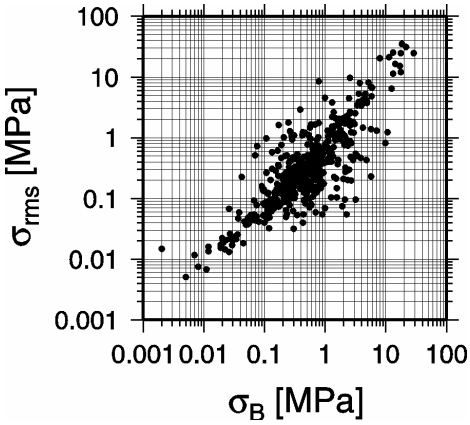

Figure 5.

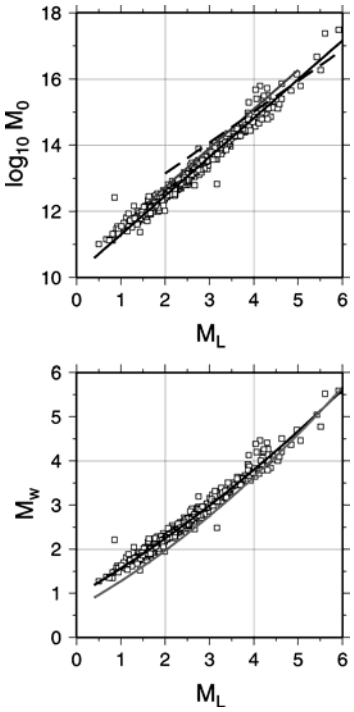

Figure 6.